Thickness Allocation Between Two Fused Silica Filters

Brian Vick and J. Robert Mahan
Mechanical Engineering Department, Virginia Tech
Blacksburg, VA 24061
Email: bvick@vt.edu
Email: jrmahan@vt.edu

and

Kory Priestley
CERES & RBI Project Scientist
NASA Langley Research Center, Science Directorate
Hampton, VA 23682
Email: kory.j.priestley@nasa.gov

ABSTRACT: The objective of this paper is to investigate the performance and effectiveness of filters used to block long-wavelength radiation in the short-wavelength channel of detectors used in earth radiation budget instruments. The detectors must respond to very low level radiation heat sources and require precise design. The advantages of a split filter are investigated. A thermal model of two-filter system is formulated. Important components of the model include the distribution of the absorbed long-wavelength radiation, obtained using the Monte-Carlo ray-trace (MCRT) method, and the radiative coupling between the filters. Results indicate that a single standard thickness filter allows far too much unwanted radiation to be re-emitted from the back surface that faces the detector. A thicker, single filter helps but is still unable to meet design criteria. It is shown that a split filter is necessary to meet the stringent design requirements usually associated with Earth radiation budget applications

INTRODUCTION

A recurring challenge in band-pass thermal radiation measurement is the management of secondary radiation emitted from the filter itself. Consider the important case of instruments, such as the "visible" channels on CERES[1] and its follow-on RBI[2], which are designed to be sensitive to radiation in the short wavelengths (near ultraviolet, visible, and near infrared). In both cited applications fused silica filters limit the channel spectral response by strongly absorbing radiation incident at wavelengths beyond about 4.0 μm while passing radiation incident at shorter wavelengths. Some of this absorbed heat is conducted to the surrounding structure and the rest is re-emitted, with approximately half of the re-emitted radiation continuing toward the detector where it is interpreted by the detector as a long-wavelength "leak" through the filter.

One way to reduce the effect of re-emitted radiation is to divide the filter into two segments. The objective of this paper is to investigate the design improvements obtained by replacing a single filter with a split filter. Parameter studies are conducted to examine the relative advantages of a two-filter system compared to the single filter arrangement.

MATHEMATICAL MODEL OF THE TWO-FILTER SYSTEM

A schematic of the filters is shown in Figure 1. Long-wave radiation is incident on the front face of filter-1. This radiation is almost completely absorbed in a thin layer near the surface, causing the back face of filter-1 to heat up by conduction. This in turn results in the heating of filter-2 by radiation exchange between the back surface of filter-1 and the front surface of filter-2. Finally, conduction causes the back face of filter-2 to heat up, resulting in unwanted secondary radiation directly to the detector.

The thermal model involves two-dimensional transient heat conduction in the radial and axial directions, as well as radiative coupling. A crucial component is the volumetric heat source $g(r,z,t)$ (W/m^3) modeling the absorbed radiation in the filter. The specific form of this heat generation is obtained from the MCRT method.

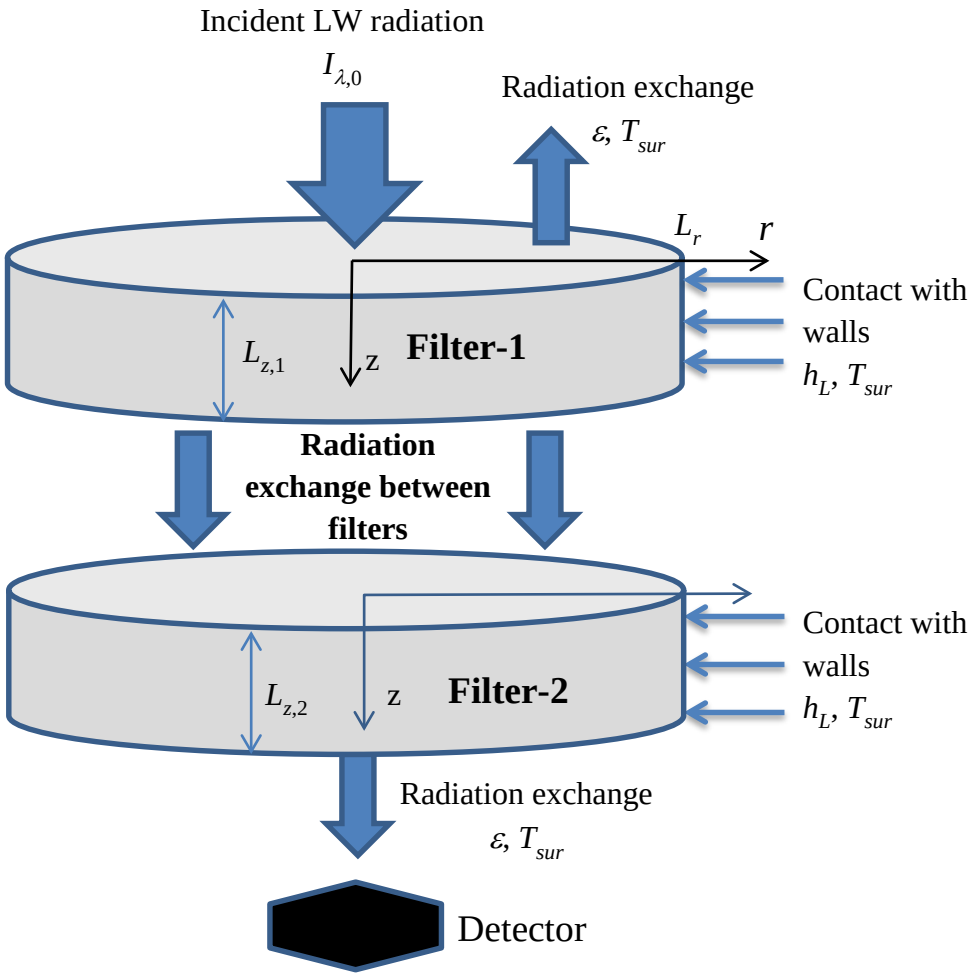

Figure 1: Schematic of the two-filter system.

***Filter*-1**

The appropriate energy equation in filter-1 is

$$\frac{\partial T_1}{\partial t} = \alpha\left(\frac{1}{r}\frac{\partial}{\partial r}\left(r\frac{\partial T_1}{\partial r}\right) + \frac{\partial^2 T_1}{\partial z^2}\right) + \frac{g_1(r,z,t)}{\rho c} \quad (1)$$

The boundary conditions are

$$\frac{\partial T_1}{\partial r} = 0 \quad , \quad r = 0 \quad (2a)$$

$$-k\frac{\partial T_1}{\partial r} = h_L\left(T_1 - T_{\infty,L}\right) \quad , \quad r = L_r \quad (2b)$$

$$-k\frac{\partial T_1}{\partial z} = \varepsilon\sigma\left(T_{sur}^4 - {T_1}^4\right) \quad , \quad z = 0 \quad (2c)$$

The parameter h_L characterizes the contact conductance between the filter and the telescope housing.

***Filter*-2**

The appropriate energy equation in filter-2 is

$$\frac{\partial T_2}{\partial t} = \alpha\left(\frac{1}{r}\frac{\partial}{\partial r}\left(r\frac{\partial T_2}{\partial r}\right) + \frac{\partial^2 T_2}{\partial z^2}\right) + \frac{g_2(r,z,t)}{\rho c} \quad (3)$$

The boundary conditions for filter-2 are

$$\frac{\partial T_2}{\partial r} = 0 \quad , \quad r = 0 \quad (4a)$$

$$-k\frac{\partial T_2}{\partial r} = h_L\left(T_2 - T_{\infty,L}\right) \quad , \quad r = L_r \quad (4b)$$

$$-k\frac{\partial T_2}{\partial z} = \varepsilon\sigma\left({T_2}^4 - T_{sur}^4\right) \quad , \quad z = L_{z,2} \quad (4c)$$

Radiative Coupling Between the Disks

$$Filter-1: \; -k\frac{\partial T_1}{\partial z} = q''_{rad,1}\left(T_1(r,L_{z,1}), T_2(r,0)\right) \quad , \quad z = L_{z,1} \quad (5a)$$

$$Filter-2: \; -k\frac{\partial T_2}{\partial z} = q''_{rad,2}\left(T_1(r,L_{z,1}), T_2(r,0)\right) \quad , \quad z = 0 \quad (5b)$$

The functions $q''_{rad,1}$ and $q''_{rad,2}$ characterize the radiation exchange between the back face of filter-1 and the front face of filter-2. They involve surface temperatures, view factors, and radiative properties. The specific details are described later.

AN APPROXIMATE ANALYSIS

Consider the two-segment filter illustrated in Figure 2. Then at equilibrium a fraction b_2 of the heat absorbed in the first segment is conducted to the surrounding structure while the remaining fraction $1 - b_2$ is re-emitted. The fraction of the radiation absorbed by the first filter that is subsequently re-emitted and absorbed by the second filter is then approximately $(1 - b_2)/2$, assuming that essentially all of the radiation emitted by the back surface of the first filter is absorbed in the second filter (worst case). Depending on the details of how the filters are mounted, it is reasonable to assume that the value of the conductance factor b_2 is proportional to the filter thickness. Therefore, if the two filter segments have the same thickness ($L_{z,1} = L_{z,2}$) then the fraction b_2 is the same for both filters. Furthermore, its value is one-half that for a single filter occupying the same space; that is $b_2 = b_1/2$. It is easy to demonstrate that the fraction of the radiation absorbed by the first filter that is subsequently emitted from the second filter toward the detector is then $\left((1 - b_2)/2\right)^2$. In the current model the value of the spacing between the two filter segments, L_{gap}, is immaterial; its only role is to prevent heat conduction between the two segments.

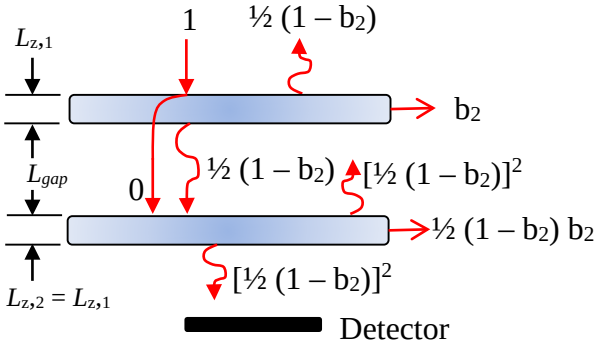

Figure 2. Split-filter model for the special case of $L_{z,1} = L_{z,2}$).

It is natural to define the *thermal effectiveness* ε of a filter as the fraction of the *absorbed* radiation that fails to pass on through. Then for a single filter $\varepsilon_1 = 1 - (1 - b_2)/2$, and for a two-segment filter, where both filters have the same thickness and occupy the same total space as the single filter, $\varepsilon_2 = 1 - \left((1 - b_2)/2\right)^2$.

Figure 3 shows the expected variation with b_1 of filter thermal effectiveness for both the single-segment filter and the double-segment filter occupying the same space (L_{gap} being negligibly small compared to $L_{z,1}$ and $L_{z,2}$). The figure shows that for the case where the filter is thermally isolated from its mounting structure ($b_1 = 0$) we can expect the split filter, with a thermal effectiveness of 0.5, to be fifty-percent more effective that the single-segment filter. However, as the fraction of the absorbed heat conducted to the mounting structure increases, the thermal effectiveness of both arrangements approaches 1.0 and the advantage of the double-segment filter over the single-segment filter diminishes, as illustrated in Figure 4.

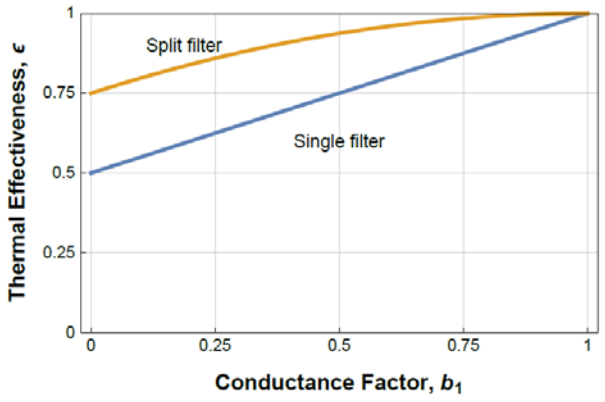

Figure 3. Comparison of thermal effectiveness of the single- and double-segment filters.

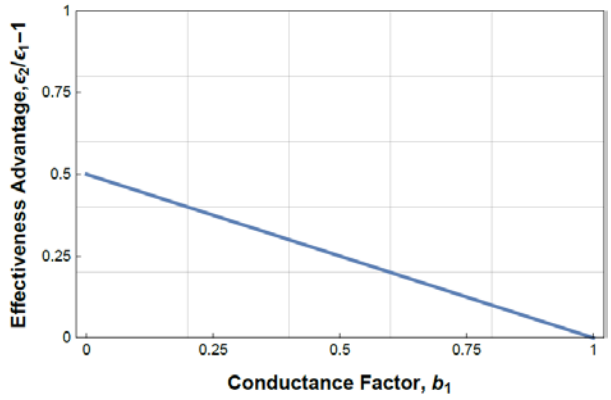

Figure 4. Effectiveness advantage of the double-segment filter over the single-segment filter.

The approximate model used to develop Figures 3 and 4 suggests two paths leading to the goal of minimizing the role of secondary emission from short-wavelength filters: (1) increasing the thickness of a single-segment filter, thereby increasing the fraction of absorbed heat conducted away to the surroundings; and (2) splitting the filter into two segments so that the second segment shields the detector from the warmer first segment. A more detailed model is required to study the distribution

of available thickness between the two segments of a split filter.

ABSORPTION OF LW EARTH-EMITTED RADIATION

The most critical input to the thermal model is the volumetric heat source, $g_1(r,z,t)$, caused by absorption of LW radiation resulting from an earth scan. In this study the Monte-Carlo ray-trace (MCRT) method is used to illuminate the front face of the short-wavelength filter arrangement. A statistically significant number of rays, typically hundreds of millions, are emitted from a black, diffuse Earth model at 308 K corresponding to an orbital altitude of 824 km. The rays are guided to the filter module of a telescope whose geometry, illustrated schematically in Figure 5, is similar to those used in CERES[1] and RBI[2]. A certain number of the rays incident to the telescope entrance aperture survive passage through the telescope baffle system and arrive at the front face of the first of two short-wavelength filter segments.

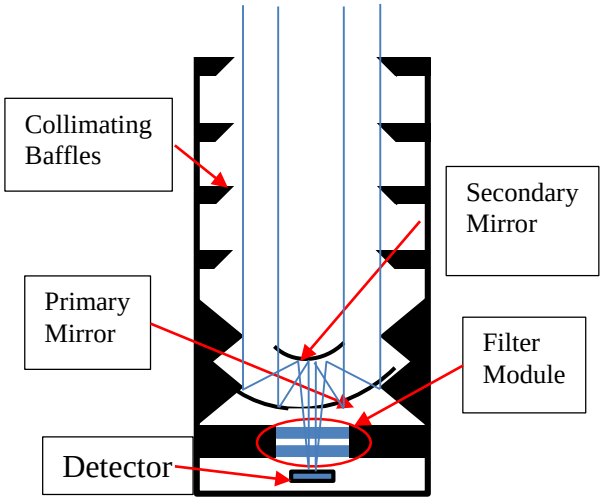

Figure 5. Schematic representation of a typical Earth radiation budget instrument.

Radiation incident to a filter is subjected to reflection at each interface, as illustrated in Figure 6. In the case of uncoated fused silica filters, about four percent of the incident radiation is reflected, while a practical anti-reflective (AR) coating can reduce this fraction to about one percent. However, the reduction in absorption within the filter due to external reflections is at least partially compensated for by internal reflections, as suggested in Figure 6. This means that for each ray incident to the filter we can consider only the absorption associated with the ray segment labeled *A* in the figure (whose relative value is assumed to be 1.0 rather than the more realistic value in the range 0.96-0.99) while still producing results relevant to the current study.

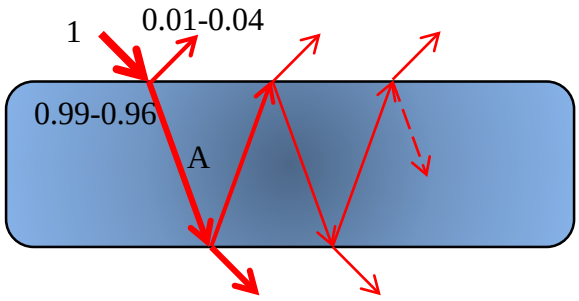

Figure 6. The disposition of radiation by a filter associated with a single incident ray.

The filter space is divided into 400 equal-volume elements on a 20-by-20 grid. The more-or-less collimated rays that make it through the telescope baffle system and are incident to the front face of the first filter (in the case of two filters) are refracted according to Snell's law,

$$\frac{sin(\theta_{in})}{sin(\theta_{ref})} = n_\lambda(\lambda). \qquad (6)$$

The exhaustive dataset for fused silica available in Kitamura, et al.[3], was used to establish models for the variation with wavelength of the refractive index n_λ and the absorption index κ_λ. The models were obtained by averaging the data in groups of ten successive wavelengths. This process leads to 192 discrete values of refractive index whose wavelength spacing is locally sufficiently dense to allow values at intermediate wavelengths to be estimated with negligible error using linear interpolation.

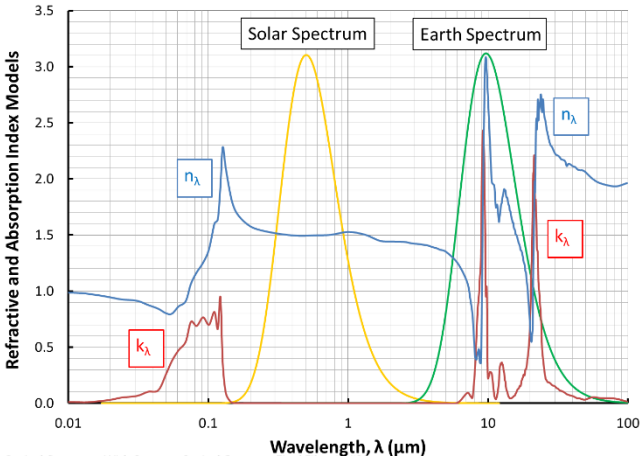

Figure 7. The variation with wavelength of the fused silica optical constants n_λ and κ_λ obtained by averaging the extensive dataset in Kitamura, et al.[3] (solar and Earth-emitted blackbody spectra are superimposed).

The area of the Earth cap subtended by the telescope in orbit is many orders of magnitude greater than the area of the telescope aperture. This means that if a normal ray

trace were employed in which rays are traced in randomly selected directions from randomly distributed locations on the Earth cap, very few if any of them would actually intersect the telescope aperture. Therefore, the rays were traced from random locations on the Earth cap to random locations on the telescope aperture. That is, if (x_E, y_E, z_E) is a random position on the Earth cap and (x_T, y_T, z_T) is a random position in the plane of the telescope service aperture, then the direction of emission is given by the direction cosines

$$L = \frac{(x_T - x_E)}{d}, M = \frac{(y_T - y_E)}{d}, N = \frac{(z_T - z_E)}{d} \quad (7)$$

where

$$d = [(x_T - x_E)^2 + (y_T - y_E)^2 + (z_T - z_E)^2]^{1/2}.$$

This approach assures that all rays emitted from the Earth cap actually intersect the telescope aperture, so that no rays are wasted, and that the spatial distribution of emission sites on the Earth cap are uniformly distributed. Each ray then carries a power of

$$P_{ray} = I_E A\Omega = (\sigma T_E^4/\pi) A_{pE}(A_{pT}/d^2) \quad (8)$$

where $A_{pE} = (A_{cap}/N_{rays})\cos\theta_E$, the projected area of the Earth source along the Earth-telescope vector of length d, and $A_{pT} = A_T\cos\theta_T$, the projected area of the telescope service aperture along the same vector.

Because of Snell's law and the wavelength dependence of the refractive index, the path through the filter of each ray is different at each wavelength. The amount of power left behind in a given cell by absorption due to a given ray and in a given wavelength interval is

$$\Delta P_\lambda = P_{inc}\left(e^{-4\pi k_\lambda L_1/\lambda} - e^{-4\pi k_\lambda L_2/\lambda}\right), \quad (9)$$

where P_{inc} is the power (W) incident to the cell boundary after the ray has traveled a distance L_1 in the filter and L_2 is the distance the ray has traveled as it exits the cell; i.e. $L_2 - L_1$ is the distance the ray has traveled through the filter. The values of n_λ and κ_λ are the mean values on the wavelength interval under consideration, computed by linear interpolation of the reflective and absorption index models shown in Figure 7. The power incident to the cell due to a given ray in the wavelength interval of interest, P_{inc}, is the fraction of the blackbody emissive power contained in that wavelength interval corresponding to the source temperature. Finally, the total power absorbed in a given cell due to all rays incident to the filter at all wavelengths between 0 and 100 μm is obtained by summing the values of ΔP_λ for that cell over rays and wavelength.

Figure 8 shows the radial distribution of absorbed power in the first two layers, each 0.05 mm thick, of the filter thickness for the case of Earth-emitted radiation. The curves for the remaining 18 layers are not shown here because they are all bunched together between the lower curve and the horizontal axis. We conclude from inspection of this figure that the filter absorbs more than 99 percent of the Earth-emitted radiation passing into it (recall that some of the incident radiation has already been reflected), and of the radiation absorbed in the filter, more than 60 percent is absorbed in the first five percent of its thickness.

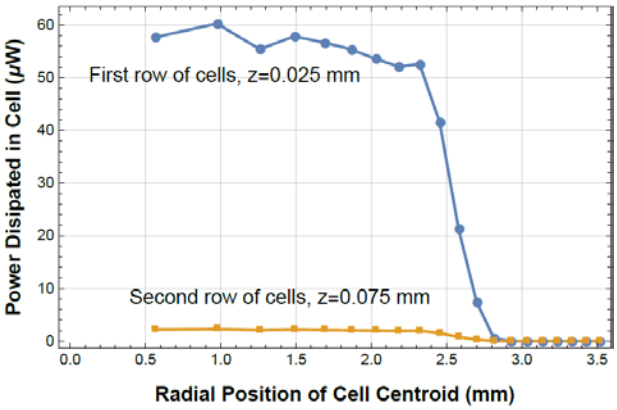

Figure 8. Distribution of absorbed LW radiation due to Earth-emitted radiation in the fused silica SW filter (Thickness = 1.0 mm, Filter Transmittance = 0.0066).

RADIATIVE COUPLING BETWEEN THE FILTERS

A critical link in the two-filter model is the radiation exchange between the two filters. In view of the fact that the surface emissivities are close to unity, combined with the relatively small gap between the surfaces, a model assuming an enclosure of black surfaces is assumed. For an enclosure of N-black surfaces, the transient energy balance at a typical surface node-i is

$$(\rho cV)_i \frac{\partial T_i}{\partial t} = -q_i = -\sum_{j=1}^{N} F_{ij} A_i (E_{b,i} - E_{b,j}) \quad (10)$$
$$= -\sum_{j=1}^{N} F_{ij} A_i \sigma (T_i^4 - T_j^4)$$

Here the F_{ij} is the traditional diffuse view factor. This expression is linearized using the radiation heat transfer coefficient as

$$(\rho cV)_i \frac{\partial T_i}{\partial t} = -\sum_{j=1}^{N} F_{ij} A_i h_{rad,ij} (T_i - T_j) \quad (11)$$

$$for\ i = 1, \ldots, N$$

where

$$h_{rad,ij} = \varepsilon\sigma(T_i^2 + T_j^2)(T_i + T_j)$$

Equation (11) is a system of N coupled, first order ODE's for the surface temperatures in the N-surface enclosure. These equations are discretized in a stable, implicit fashion as

$$(\rho cV)_i \frac{T_i^{p+1} - T_i^p}{\Delta t} = -\sum_{j=1}^{N} F_{ij} A_i h_{rad,ij}^p \left(T_i^{p+1} - T_j^{p+1}\right) \quad (12)$$

or

$$T_i^{p+1} - T_i^p = -\sum_{j=1}^{N} U_{ij}^p \left(T_i^{p+1} - T_j^{p+1}\right) \quad (13)$$

where

$$U_{ij}^p = \Delta t \frac{F_{ij} A_i h_{rad,ij}^p}{(\rho cV)_i}$$

The matrix form of Equation (13) is

$$[\bar{\boldsymbol{I}} + \overline{\boldsymbol{W}}]\bar{\boldsymbol{T}}^{p+1} = \bar{\boldsymbol{T}}^p \quad (14)$$

$$\bar{\boldsymbol{T}}^p = \begin{bmatrix} T_1^p \\ \vdots \\ T_i^p \\ \vdots \\ T_N^p \end{bmatrix}, \quad \overline{\boldsymbol{W}} = \begin{bmatrix} W_{11} & \cdots & W_{1N} \\ \cdots & W_{ij} & \\ & & \ddots \end{bmatrix}$$

$$W_{ij} = \begin{cases} \left(\sum_{k=1}^{N} U_{ik}\right) - U_{ii} & , \quad j = i \\ -U_{ij} & , \quad j \neq i \end{cases}$$

Equation (14) provides the rule governing the temperature change at each time step due to radiation exchange between the surface cells on the back surface of filter-1 and the front surface of filter-2.

NUMERICAL SOLUTION

In this paper, the complex model building procedure developed by Vick[4] is applied to the multi-dimensional, two filter model. The complete mathematical model is defined by Equations (1)-(5) and consists of a combination of individual processes. The method is referred to as a modified cellular automata method, since each ingredient is handled in a discrete, individual manner. The relevant processes are executed in the following sequence.

1. Filter-1: Volumetric source caused by absorption of LW radiation, characterized by the function $g_1(r, z, t)$.
2. Filter-1: Boundary interaction at $r = L_r$ due to contact conduction between the filter and the support.
3. Filter-1: Boundary interaction at the exposed front boundary at z=0 due to radiative exchange with the telescope.
4. Filter-1: Heat conduction in the *r*-direction.
5. Filter-1: Heat conduction in the *z*-direction.
6. Radiative coupling between filters 1and 2.
7. Filter-2: Volumetric source caused by absorption of LW radiation, characterized by the function $g_2(r, z, t)$.
8. Filter-2: Boundary interaction at $r = L_r$ due to contact conduction between the filter and the support.
9. Filter-2: Boundary interaction at the exposed back boundary at $z = L_{z,2}$ due to radiative exchange with the telescope.
10. Filter-2: Heat conduction in the *r*-direction.
11. Filter-2: Heat conduction in the *z*-direction.

Each of these processes is solved in a numerically stable and efficient way. From these elementary processes, the entire model is assembled. The details of the algorithms for solving for volumetric heat sources, heat conduction in cylindrical coordinates, heat conduction on rectangular coordinates, and boundary interactions were described in detail in reference [4].

FILTER RESULTS

The parameters used in the current simulation are listed in Table 1. The mathematical model defined by Equations (1)-(5) were solved using the modified cellular automata method[4].

Table 1: Parameters used in the SW filter test cases.

	Symbol	*Units*	*Value*
Geometry	L_r	mm	5
	L_z	mm	1
	$L_{z,1}$	mm	0.5
	$L_{z,2}$	mm	0.5
Thermal Properties: fused silica	ρ	kg/m^3	2180
	c	J/kg·K	750
	k	W/m·K	1.38
Boundary at $r = L_r$	h_L	W/m^2·K	75,000
	$T_{\infty,L}$	K	308
Boundaries at $z = 0$ and L_z	ε	-	1
	T_{sur}	K	308
Volumetric heat source	g	W/m^3	MCRT
Initial condition	T_0	K	308

The basic thermal response of the split filter is shown in Figures 9a,b. The steady-state temperature distributions at the 4 surfaces are shown in Figure 9a while the transient response at the center of these 4 surfaces are shown in Figure 9b. The front surface of filter-1, where most of the LW radiation is absorbed, is the hottest with only a small drop in temperature at the back surface of filter-1. However, the second filter is significantly cooler. The reason is that by splitting the filter, the relatively strong heat conduction mechanism to filter-2 has been completely eliminated. In its place is a relatively weak mechanism due to radiation exchange across a small temperature difference. Here lies the fundamental reason that a two-filter system is effective.

The important result is the back surface of filter-2, since the extremely sensitive detector is directly exposed to this surface, as seen in Figure 1. A design criteria analysis of the noise equivalent power level indicated that the temperature rise design limit of the back surface of filter-2 should be no more than 9 mK. The split filter arrangement is able to satisfy that criteria.

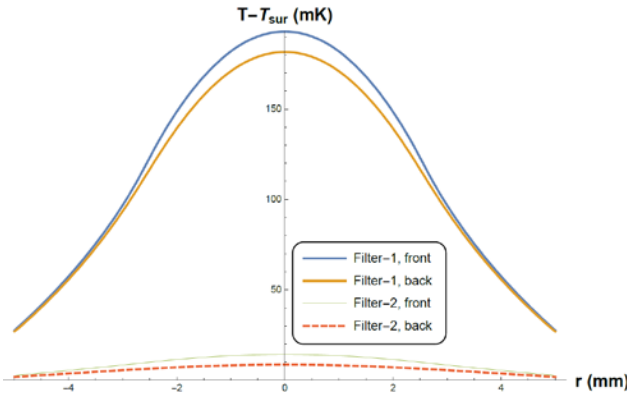

Figure 9a: Steady state temperature rise at the surfaces of the split filter.

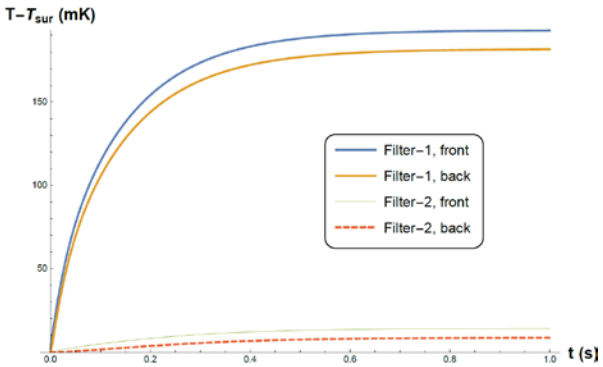

Figure 9b: Transient temperature rise at the center of the surfaces for the split filter.

Next, Figures 10a,b,c are presented to show the advantage of using a split filter and a thicker, single filter. Comparison with a standard single filter of nominal thickness L_z = 1 mm is shown. The use a thicker single filter of 2 mm thickness reduces the temperature rise by a factor of about 2, but is not able to meet the design criteria of a 9 mK temperature rise. However, splitting a filter into two disks each of thickness 0.5 mm is much more effective in keeping the back surface cool, thus reducing the unwanted secondary emission to the detector and meeting the design criteria.

Figure 10c shows the thermal effectiveness, defined as the fraction of absorbed radiation that fails to get through the filter. Although a single filter is able to block over 96% of the LW radiation, the 4% that reaches the back surface causes too much unwanted noise on the sensitive detector. The split filter is able to block over 99% of the undesired emission. This level of precision is necessary in the current application.

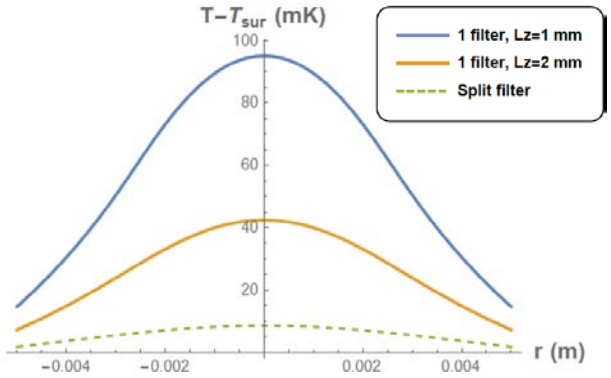

Figure 10a: Steady state temperature rise over the back surface for one filter and split filters ($L_{z,1} = L_{z,2} = 0.5\ mm$).

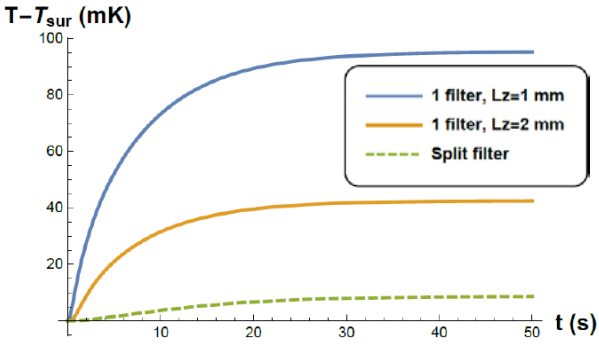

Figure 10b: Transient temperature rise at the center of the back surface for one filter and split filters.

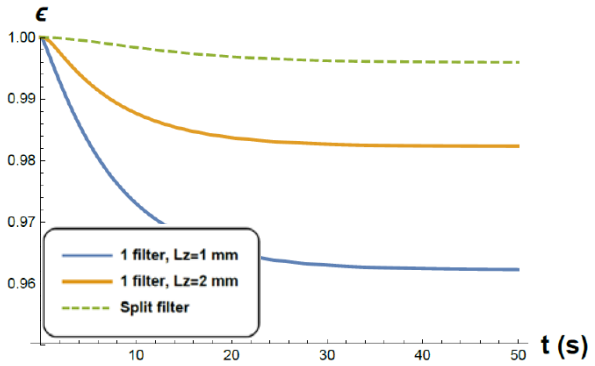

Figure 10c: Thermal effectiveness for one filter and split filters.

Figures 11a and 11b show the effect of splitting a single filter of thickness 1 mm into two filters with the same total thickness. Thus a 10/90 filter has dimensions $L_{z,1} = 0.1\ mm$ and $L_{z,2} = 0.9\ mm$. Interestingly the 50/50 split produces the lowest temperatures and is the optimum choice. A 75/25 split produces somewhat higher temperatures that slightly exceed the design limit in the filter center. Lastly, the 10/90 and 90/10 cases produced results that were very close to one another and appear as a single curve on the scale used. The temperatures for this uneven split are significantly too high. Figure 11b shows that a very high effectiveness of at least 99.7% is required for this sensitive application.

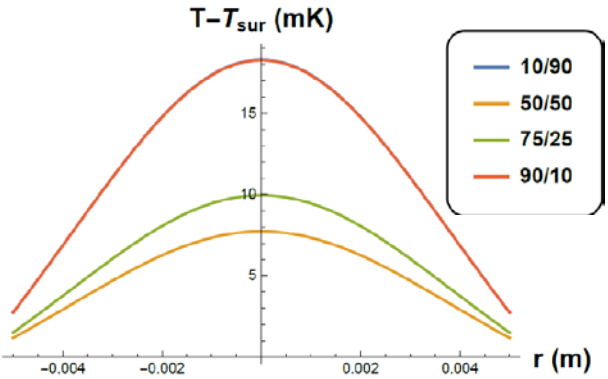

Figure 11a: Steady state temperature rise over the back surface.

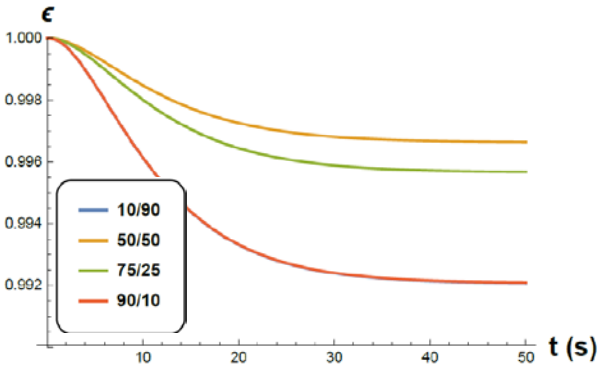

Figure 11b: Thermal effectiveness.

SUMMARY and CONCLUSIONS

- A thermal model of a two-filter system is formulated. Important components include
  - The distribution of the absorbed LW radiation, obtained using the MCRT method
  - The radiative coupling between the filters
- A *Modified Cellular Automata* technique is used to build complex models from simple processes. This technique is being extended to build a compete end-to-end model of the telescope.
- Results indicate that
  - A single standard thickness filter allows far too much unwanted radiation to be re-emitted to the detector.
  - A thicker, single filter helps but is still unable to meet design criteria.
  - A split filter is necessary to meet the stringent design requirements associated with Earth radiation budget applications.

REFERENCES

1. B. A. Wielicki, R. D. Cess, M. D. King, D. A. Randall, and E. F. Harrison, "Mission to Planet Earth: Role of Clouds and Radiation in Climate," Bulletin of the American Meteorological Society, Vol. 76, No. 11, November 1995, pp. 2125-2153.c
2. Elena Georgieva, Kory J. Priestley, Barry Dunn, Richard Cageao, Anum Barki, Jim Osmundsen, Craig Turczynski, and Nurul Abedin, "Radiation Budget Instrument (RBI) for JPSS-2," 24th Conference on Characterization and Radiometric Calibration for Remote Sensing (CALCON), Space Dynamics Laboratory, Utah State University, Logan, UT, August 20-24, 2015.
3. R. Kitamura, L. Pilon, and M. Jonasz, "Optical Constants of Silica Glass from Extreme Ultraviolet to Far Infrared at Near Room Temperatures, **Applied Optics**, Vol. 46, No. 33, 20 November 2007.
4. Vick, B., 2007, "Multi-Physics Modeling Using Cellular Automata," *Complex Systems*, Vol. 17 (1 & 2), pp. 65-78.